

Superconducting properties and Fermi-surface topology of the quasi-two-dimensional organic superconductor λ -(BETS)₂GaCl₄ (BETS \equiv bis(ethylene-dithio)tetraselenafulvalene)

Charles Mielke^{1,5}, John Singleton^{1,2}, Moon-Sun Nam², Neil Harrison¹,
C C Agosta³, B Fravel⁴ and L K Montgomery⁴

¹ National High Magnetic Field Laboratory, Los Alamos National Laboratory, MS-E536,
Los Alamos, NM 87545, USA

² University of Oxford, Department of Physics, The Clarendon Laboratory, Parks Road,
Oxford OX1 3PU, UK

³ Department of Physics, Clark University, Worcester, MA 01610, USA

⁴ Department of Chemistry, Indiana University, Bloomington, IN 47405, USA

E-mail: cmielke@lanl.gov (C Mielke)

Received 3 April 2001, in final form 30 July 2001

Published 23 August 2001

Online at stacks.iop.org/JPhysCM/13/8325

Abstract

The Fermi-surface topology of the organic superconductor λ -(BETS)₂GaCl₄ has been determined using the Shubnikov–de Haas and magnetic breakdown effects and angle-dependent magnetoresistance oscillations. The former experiments were carried out in pulsed fields of up to 60 T, whereas the latter employed quasistatic fields of up to 30 T. All of these data show that the Fermi-surface topology of λ -(BETS)₂GaCl₄ is very similar to that of the most heavily studied organic superconductor, κ -(BEDT-TTF)₂Cu(NCS)₂ (BEDT-TTF \equiv bis(ethylene-dithio)tetrathiafulvalene), except in one important respect: the interplane transfer integral of λ -(BETS)₂GaCl₄ is a factor ~ 5 larger than that of κ -(BEDT-TTF)₂Cu(NCS)₂. The increased three-dimensionality of λ -(BETS)₂GaCl₄ is manifested in radio-frequency penetration-depth measurements, which show a clear dimensional crossover in the behaviour of $H_{c2}(T)$. The radio-frequency measurements have also been used to extract the Labusch parameter determining the fluxoid interactions as a function of temperature, and to map the flux-lattice melting curve.

(Some figures in this article are in colour only in the electronic version)

⁵ Author to whom any correspondence should be addressed.

1. Introduction

There is considerable current debate over the nature of superconductivity in quasi-two-dimensional (Q2D) crystalline organic metals [1–4]. The most heavily studied members of this family of materials are the κ -phase BEDT-TTF salts (e.g. κ -(BEDT-TTF)₂Cu(NCS)₂) [1]. Whilst nuclear magnetic resonance [5], penetration-depth [2], tunnelling [4] and other experiments [1] appear to suggest that the superconductivity in these salts may be d-wave-like and mediated by spin-density-wave-like fluctuations, some doubts have been cast by recent controversial specific heat measurements, which may suggest that the order parameter does not possess the required nodes [3]. Several theories [6–9] stress the importance of the details of the Fermi-surface topology in providing suitable prerequisites for superconductivity; if the Fermi-surface geometry and interactions are altered slightly, it appears that BCS-like s-wave superconductivity *may* be the dominant low-temperature ground state [1].

Clearly, it is of importance to study organic superconductors with slight variations in Fermi-surface topology so that the effect on the superconducting ground state can be assessed. In this paper we therefore report magnetotransport and radio-frequency penetration-depth measurements of the superconductor λ -(BETS)₂GaCl₄. Shubnikov–de Haas oscillations, magnetic breakdown and angle-dependent magnetoresistance oscillations indicate that the effective masses of λ -(BETS)₂GaCl₄ and much of the topology of its Fermi surface are similar to those of the most heavily studied BEDT-TTF superconductor, κ -(BEDT-TTF)₂Cu(NCS)₂. However, the magnetoresistance close to $\theta = 90^\circ$ implies that the interplane transfer integral in λ -(BETS)₂GaCl₄ is approximately five times larger than that in κ -(BEDT-TTF)₂Cu(NCS)₂, suggesting that λ -(BETS)₂GaCl₄ is less two-dimensional. This increased dimensionality is manifested in the superconducting properties of λ -(BETS)₂GaCl₄; a clear two-dimensional–three-dimensional crossover is seen in the temperature dependence of H_{c2} . We have also used the radio-frequency measurements to extract various parameters related to the interactions between the fluxoids and to reveal the melting of the vortex solid.

2. Background information

When the innermost four sulphur atoms of BEDT-TTF [1] are replaced by selenium to produce BETS (where BETS stands for bis(ethylene-dithio)tetraselenafulvalene), electrocrystallization gives rise to a range of charge-transfer salts with notably different properties compared to their BEDT-TTF counterparts [10–13]. Salts of the λ -phase morphology are currently unique to the BETS series, and λ -(BETS)₂GaCl₄ ($T_c \approx 5$ K) remains the only superconducting BETS charge-transfer salt found thus far [12, 14].

Crystals of the λ -phase exist in the form of needles with the long axis of the needle corresponding to the shortest lattice vector c [11, 12]. At first sight, the crystal structure looks quasi-one-dimensional, with the BETS molecules packing roughly parallel in the planes between the anions [12]. However, the BETS sites are not equivalent, and the cation molecules in fact occur in dimers, surrounded roughly isotropically by four nearest-neighbour dimers with the same orientation. The crystallographic unit cell contains two dimers, and hence contributes two holes [12]. Although the details of the cation positioning and symmetry are rather different to those for κ -(BEDT-TTF)₂Cu(NCS)₂ [1], the overall similarity of the dimer arrangements leads one to expect a Fermi surface for λ -(BETS)₂GaCl₄ which is topologically similar to that in κ -(BEDT-TTF)₂Cu(NCS)₂. Indeed, the calculated band structure of λ -(BETS)₂GaCl₄ predicts a Fermi surface consisting of a quasi-two-dimensional (Q2D) hole pocket (the α -pocket) and a pair of warped quasi-one-dimensional (Q1D) sheets [12, 15]. According to the calculations, the α -pocket in this case is expected to occupy ~ 28 – 33% of the Brillouin zone [12, 15].

3. Magnetotransport studies

3.1. Experimental details

Single crystals of approximate dimensions $1 \times 0.1 \times 0.05 \text{ mm}^3$ were synthesized using electrochemical techniques [12] employing a 1, 1-trichloroethane/1, 1, 2-trichloroethane/ethanol solvent system [16]. For the purpose of performing four-wire resistance measurements, 12 μm gold leads were attached to the samples using graphite paint. In the pulsed-field experiments, the resistance was measured using a 10 μA ac current with a frequency of 200 kHz [1, 17]. The voltage was measured using a high-speed lock-in amplifier. Temperatures as low as $\sim 340 \text{ mK}$ were achieved by immersing the sample in liquid ^3He inside a plastic cryostat [17]. Capacitor-driven, ~ 40 -millisecond-duration pulsed magnetic fields of up to 60 T were provided by the National High Magnetic Field Laboratory (NHMFL), Los Alamos. Angle-dependent magnetoresistance (AMRO) studies were made using a two-axis rotation insert [1] in quasistatic magnetic fields of up to 30 T provided by NHMFL, Tallahassee. In the AMRO experiments, an ac current of 5 μA (frequency 30–80 Hz) was used for the resistance measurements, and a stable base temperature of 1.4 K was obtained by pumping on ^4He liquid. In both pulsed and quasistatic measurements, the current through the sample was driven in the interplane b^* -direction; in such a configuration the measured resistance is accurately proportional to the interplane resistivity component ρ_{zz} [1].

3.2. Pulsed-field magnetotransport: Shubnikov–de Haas and magnetic breakdown oscillations

Figure 1 shows the magnetoresistance of a λ -(BETS)₂GaCl₄ crystal obtained using pulsed magnetic fields; the temperature was 340 mK and the magnetic field was applied parallel to the b^* -direction (i.e. perpendicular to the Q2D planes of the crystal) [11]. After the superconducting-to-normal transition, the resistance rises until a series of low-frequency Shubnikov–de Haas oscillations emerges at about 33 T. These grow in amplitude, until at about 45 T, a higher-frequency series of oscillations becomes visible. The inset shows a Fourier transform of the magnetoresistance data. The lower of the two frequencies F_α (believed to originate from the α -pocket) is $650 \pm 5 \text{ T}$. The higher frequency of $4030 \pm 25 \text{ T}$, which occurs at fields above $\sim 45 \text{ T}$, corresponds to an area in k -space approximately equal to the Brillouin-zone cross-section; following common usage for other charge-transfer salts [1], we will refer to this as the β -frequency F_β . Frequencies equivalent to the Brillouin-zone area are readily observed in other charge-transfer salts (typically in κ - and α -phase salts of the form (BEDT-TTF)₂X) as a result of magnetic breakdown, whereby electrons tunnel between the Q1D and Q2D sections of the Fermi surface [1].

The observation of magnetic breakdown in this material is not unexpected, given the small size of the gap between the Q2D and Q1D Fermi-surface sections predicted by the band-structure calculations [12]. However, the experimentally observed value of $F_\alpha \approx 650 \text{ T}$ is roughly a factor two smaller than that predicted by the calculations. Discrepancies between model and experiment of this size are not unknown in charge-transfer salts [18, 19].

3.3. Effective-mass determination

Although the Fermi surface of λ -(BETS)₂GaCl₄ is Q2D, the relatively small amplitudes of the oscillations in the magnetoresistance (see figure 1) and the absence of harmonics in the Fourier transform (inset to figure 1) imply that the Lifshitz–Kosevich (LK) theory should provide an

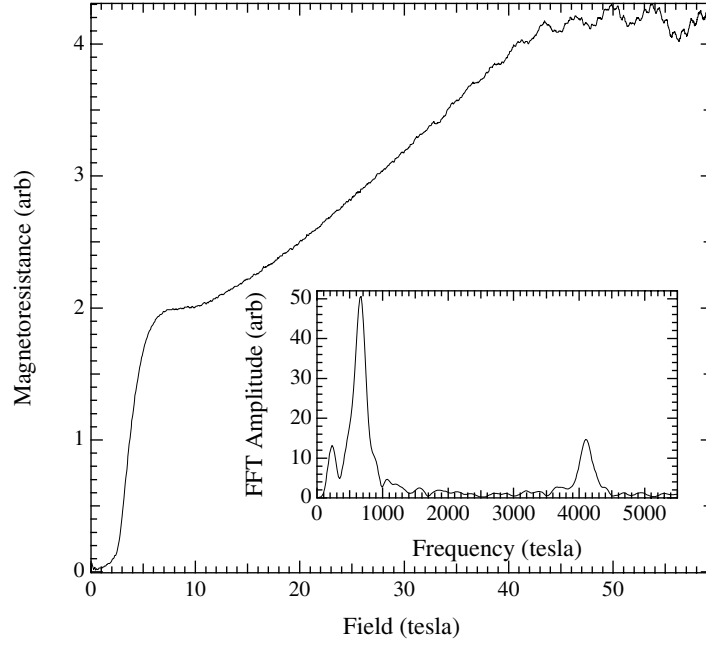


Figure 1. Resistance of a λ -(BETS) $_2$ GaCl $_4$ crystal as a function of magnetic field, applied parallel to the b^* -direction; the temperature is 340 mK. The inset shows a Fourier transform of the data after subtraction of the non-oscillatory background [1]. The peak at 650 T is associated with the α -pocket; that at 4030 T is due to the breakdown (β -) orbit which encompasses 100% of the Brillouin zone.

accurate description of the temperature dependence of the oscillations [1]. According to this theory, the thermal damping factor has the form [20]

$$R_T(B, T) = \frac{\chi(m^*/m_e)T/B}{\sinh(\chi(m^*/m_e)T/B)} \quad (1)$$

where $\chi = 14.69 \text{ T K}^{-1}$ and m_e is the free-electron mass. On fitting the amplitudes of the oscillations as a function of temperature (14 different temperatures ranging from 340 mK to 3.0 K were used), we obtain the effective masses $m_\alpha^* = 3.6 \pm 0.1 m_e$ for F_α and $m_\beta^* = 6.3 \pm 1 m_e$ for F_β .

Table 1 compares the effective masses and the Fermi-surface areas obtained for λ -(BETS) $_2$ GaCl $_4$ and the most heavily studied κ -phase BEDT-TTF superconductor, κ -(BEDT-TTF) $_2$ Cu(NCS) $_2$ [21] (see section 3.2 of reference [1] for similar data on other κ -phase BEDT-TTF salts). Note that the Fermi-surface parameters of the two salts are remarkably similar. Moreover, band-structure calculations for both salts predict $m_\alpha^* \sim m_e$ [12, 21], whereas the observed masses are a factor ~ 3.5 bigger than this, indicating that interactions which renormalize the quasiparticle masses [1, 21, 22] are of similar importance in the two materials. In both cases, the band-structure calculations [12, 21] predict that $m_\beta^* \approx 2m_\alpha^*$, in reasonable agreement with the experimental values, and suggesting that the renormalizing interactions influence both Q1D and Q2D Fermi-surface sections in a similar manner [1, 21]. The only marked difference between λ -(BETS) $_2$ GaCl $_4$ and κ -(BEDT-TTF) $_2$ Cu(NCS) $_2$ is the relatively high value of the Dingle temperature in the former material; the rate of growth of the oscillations with increasing field (see figure 1) suggests a Dingle temperature of $T_D \approx 3.2 \pm 0.1 \text{ K}$ for the α -pocket. Typical values of T_D for κ -(BEDT-TTF) $_2$ Cu(NCS) $_2$ crystals [1, 23] (and indeed

Table 1. Comparison of magnetic quantum oscillation frequencies and effective masses in λ -(BETS)₂GaCl₄ and κ -(BEDT-TTF)₂Cu(NCS)₂. The table shows the effective masses m_α^* and m_β^* and frequencies F_α and F_β corresponding to the α - and β -orbits of the Fermi surface.

Salt	m_α^*/m_e	F_α (T)	m_β^*/m_e	F_β (T)	T_c (K)	Source
κ -(BEDT-TTF) ₂ Cu(NCS) ₂	3.5	600	6.5	3920	10.4	[21]
λ -(BETS) ₂ GaCl ₄	3.6	650	6.3	4030	5	Present work

κ -phase BETS salts [24]) are often a factor ~ 5 smaller than this, indicating that the impurity scattering rate in λ -(BETS)₂GaCl₄ is relatively high. The reason for this difference is not yet clear.

3.4. Angle-dependent magnetoresistance oscillations (AMROs)

Figure 2(a) shows the magnetoresistance of a λ -(BETS)₂GaCl₄ crystal as a function of θ , the angle between the applied magnetic field and b^* . Data are shown for a number of different

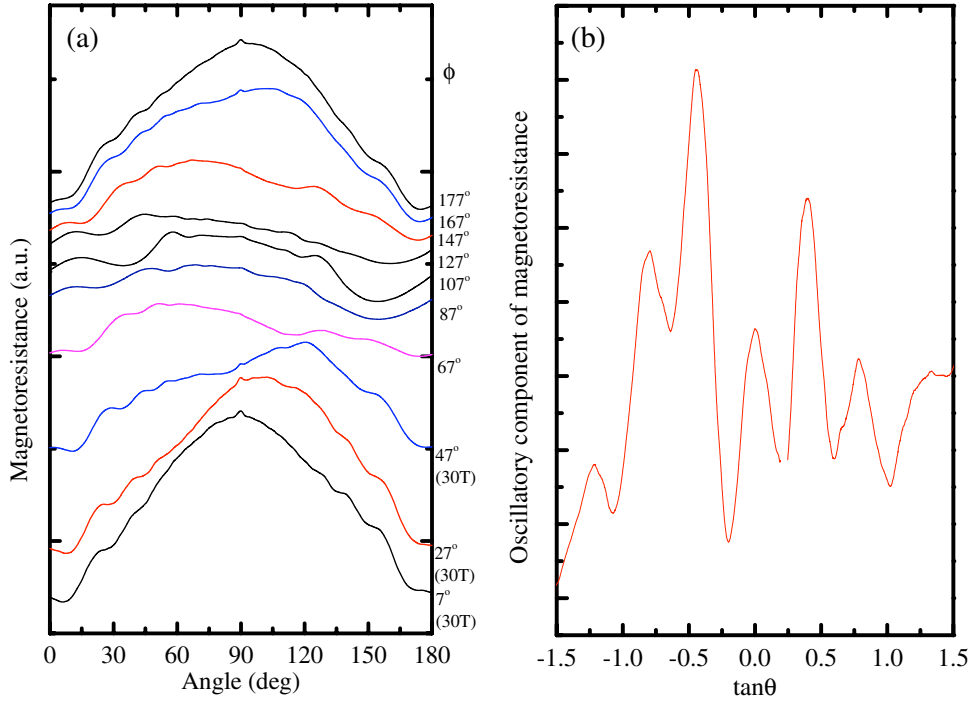


Figure 2. (a) Magnetoresistance of a λ -(BETS)₂GaCl₄ crystal as a function of θ , the angle between the applied magnetic field and b^* . Data are shown for a number of different ϕ -angles (listed on the right of the figure), where ϕ is azimuthal angle between the plane of rotation and the b^*c -plane. The lowest three traces were recorded at 30 T; the rest of the data were acquired at 27 T. AMROs are observed as gentle oscillations of the resistance, periodic in $\tan \theta$; the small peak at 90° is due to the presence of a small number of closed quasiparticle orbits on the warped Fermi-surface sections. (b) An illustration of the method of locating the AMRO resistance maxima ($\phi = 7^\circ$ data from (a)). The slowly varying background magnetoresistance has been fitted to a fourth-order polynomial in θ and subtracted from the experimental data, leaving the oscillatory component. Peaks periodic in $\tan \theta$ are plainly visible.

ϕ -angles, where ϕ is the azimuthal angle between the plane of rotation and the $\mathbf{b}^*\mathbf{c}$ -plane. Distinct AMROs are observed; their ϕ -dependence suggests that they are caused by a Q2D Fermi-surface section [1, 19]. In such a case, maxima in the magnetoresistance occur at angles θ_i defined by [1, 19]

$$b'k_{\parallel} \tan \theta_i = \pi \left(i \pm \frac{1}{4} \right) + A(\phi) \quad (2)$$

where i is an integer, k_{\parallel} is the maximum Fermi-wave-vector projection on the plane of rotation of the field and b' is the effective interplane spacing (see figure 2(b)). On plotting the positions of the maxima θ_i versus i , taking account of the correct sign of the $\pi/4$ term [18, 19], we obtain straight lines at all azimuthal angles in accordance with these expectations. On choosing b' to be the interlayer spacing (18.4 Å) obtained from x-ray diffraction studies [12, 15], we obtain the locus for k_{\parallel} versus ϕ shown in figure 3(a).

A locus in the shape of a figure of eight is the usual result for a pocket of elliptical cross-section [1, 18, 19]. For a pocket of ideal elliptical geometry, the locus of k_{\parallel} is given by

$$k_{\parallel} = [k_x^2 \cos^2(\phi - \xi_{\text{inc}}) + k_y^2 \sin^2(\phi - \xi_{\text{inc}})]^{1/2} \quad (3)$$

where ξ_{inc} is the inclination of the major axis of the ellipse with respect to the $\mathbf{b}^*\mathbf{c}$ -plane. The parameters $k_x = 4.86 \pm 0.08 \text{ nm}^{-1}$, $k_y = 1.63 \pm 0.01 \text{ nm}^{-1}$ and $\xi_{\text{inc}} = 19^\circ \pm 5^\circ$ yield the best fit (solid curves in figure 3(a)).

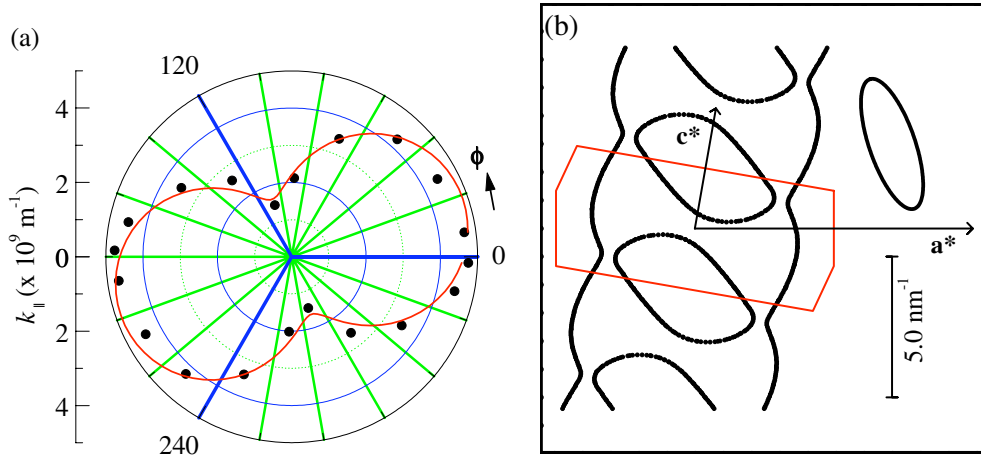


Figure 3. (a) The locus of k_{\parallel} versus azimuthal angle ϕ derived from fits of equation (2) to the AMRO data. Data are points and the curve is a fit to equation (3) with the parameters $k_x = 4.86 \pm 0.08 \text{ nm}^{-1}$, $k_y = 1.63 \pm 0.01 \text{ nm}^{-1}$, $\xi_{\text{inc}} = 19^\circ \pm 5^\circ$ and $b' = 18.4 \text{ \AA}$. (b) The experimental cross-sectional shape and orientation of the Q2D Fermi-surface pocket, shown alongside (and to the same scale as) the Brillouin zone, reciprocal-lattice vectors \mathbf{a}^* , \mathbf{c}^* and calculated Fermi surface of reference [15]. The pocket is described by the parameters $k_x = 2.43 \pm 0.04 \text{ nm}^{-1}$, $k_y = 0.815 \pm 0.005 \text{ nm}^{-1}$, $\xi_{\text{inc}} = 19^\circ \pm 5^\circ$ and $b' = 2 \times 18.4 \text{ \AA} \approx 36.8 \text{ \AA}$ (see the text and equation (3)).

The values of k_x and k_y deduced from the AMRO data indicate an ellipse area corresponding to a Shubnikov–de Haas frequency of $2608 \pm 60 \text{ T}$. This is almost exactly four times larger than the value of F_α observed for λ -(BETS)₂GaCl₄ (see table 1). It is inconceivable that this value of $\sim 2608 \text{ T}$ could be the actual area of the α -pocket, as it would then occupy $\sim 66\%$ of the Brillouin zone. Quantum oscillation measurements remain the definitive method for obtaining Fermi-surface cross-section areas [1, 20]. On the other hand, the AMRO measurements shown in figure 2 behave exactly as one would expect for a Q2D

Fermi-surface pocket [19], with no evidence for any significant misalignment of the sample; i.e. the fits to equation (2) are straight lines and the peak feature at $\theta \approx 90^\circ$ occurs at 90° for all azimuthal angles.

A possible explanation is that the true interlayer spacing (as perceived by the quasiparticles) is double the unit-cell height, or that there is a modulation of the lattice in the crystallographic b -direction; this would result in an effective interlayer spacing of $b' = 2 \times 18.4 \text{ \AA} \approx 36.8 \text{ \AA}$. Such a modulation of the lattice could occur in the event of a charge-density-wave (CDW) or spin-density-wave (SDW) instability; however, there is as yet no other evidence for the presence of such a ground state (cf. numerous other charge-transfer salts in which CDWs or SDWs cause extensive modification of the quantum oscillation spectrum [1, 25]). If such a modulation exists, it is too weak to be picked up by a careful x-ray study at 115 K (Bruker-AXS SMART6000 CCD, complete sphere of data, sixty-second frames, 0.3° scans) [26]. However, this does not rule out the possibility that doubling occurs at a lower temperature [26].

Whatever the mechanism, a doubling of b' (see equation (2)) would result in the Fermi-surface parameters $k_x = 2.43 \pm 0.04 \text{ nm}^{-1}$, $k_y = 0.815 \pm 0.005 \text{ nm}^{-1}$ and $\xi_{\text{inc}} = 19^\circ \pm 5^\circ$ yielding an ellipse area corresponding to a Shubnikov–de Haas frequency of $652 \pm 15 \text{ T}$, in very good agreement with $F_\alpha = 650 \pm 5 \text{ T}$ derived in section 3.2. Figure 3(b) shows an elliptical-cross-section Q2D pocket of this size and orientation alongside the most recent calculation of the Fermi surface [15], based on structural studies carried out at 17 K. The Q2D pocket measured experimentally is smaller and somewhat more elongated than that suggested by the calculations; it occupies $\approx 16\%$ of the Brillouin zone, whereas the Q2D pocket of the calculation is 28% of the Brillouin-zone area. However, such discrepancies between calculation and experiment are not without precedent in crystalline organic metals [18, 19, 25].

3.5. Estimation of the interplane transfer integral

We now turn to the small peak in the magnetoresistance component ρ_{zz} observed at $\theta = 90^\circ$ in figure 2. Thus far, we have treated only the Fermi-surface cross-section in the a^*c^* -plane (see figure 3(b)). However, a small, but finite interlayer transfer integral will lead to a warping of the Fermi surface in the interlayer b^* -direction (see section 2 of reference [1]). When the magnetic field is almost exactly in the plane of the warping, a few closed orbits become possible on the warped sections of the Fermi surface (e.g. on the ‘bellies’ of the warped Q2D Fermi cylinders) [27, 28, 30]. For certain orientations of an in-plane field, closed orbits will be possible on both the Q1D sheets and Q2D cylinders of a Fermi surface such as that shown in figure 3(b); at other orientations of an in-plane field, only the Q2D cylinders will be able to support closed orbits on their bellies. Such orbits are very effective at averaging the interplane velocity component v_z , and hence lead to a peak in ρ_{zz} [28–30].

As the magnetic field is tilted away from the in-plane direction ($\theta = 90^\circ$), the closed orbits will cease to be possible when $\theta = 90^\circ \pm \Delta$, where the angle Δ is given by

$$\Delta \text{ (in radians)} \approx \frac{v_\perp}{v_\parallel} \quad (4)$$

where v_\perp is the maximum interlayer quasiparticle velocity and v_\parallel is the intralayer component of the quasiparticle velocity in the plane of rotation of the magnetic field [28–30]. If the quasiparticle dispersion $E(k_b)$ in the interlayer direction is assumed to follow a simple tight-binding model, $E(k_b) = -2t_\perp \cos(k_b b)$ [31], where t_\perp is the interlayer transfer integral, then

$$v_\perp = 2t_\perp b / \hbar \quad (5)$$

where we have used the relationship $\hbar v = \nabla_k E(k)$ [31] to obtain v_\perp from $E(k_b)$ [30]. Equations (4) and (5) therefore show that there is a direct proportionality between 2Δ , the angular width of the peak in ρ_{zz} , and the interlayer transfer integral, t_\perp .

Figure 4 shows how the angular width 2Δ of the peak in ρ_{zz} is defined; the limits of the peak are defined by the intersections of extrapolations of the background magnetoresistance and the edges of the peak⁶. Similar data for κ -(BEDT-TTF)₂Cu(NCS)₂ from reference [30] are plotted for comparison; note how the peak at 90° is much narrower. Given the similarity of their intralayer Fermi-surface properties (see table 1), this comparison immediately suggests a much smaller t_\perp in κ -(BEDT-TTF)₂Cu(NCS)₂ than in λ -(BETS)₂GaCl₄.

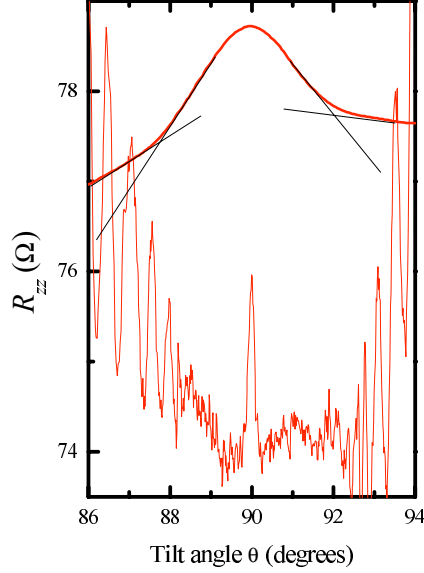


Figure 4. Peaks in the interplane resistance R_{zz} (proportional to ρ_{zz}) close to $\theta = 90^\circ$ in λ -(BETS)₂GaCl₄ (thick line; $T = 1.4$ K, $B = 30$ T; present work) and κ -(BEDT-TTF)₂Cu(NCS)₂ (fine line; $T = 520$ mK, $B = 42$ T; reference [30]). In the case of κ -(BEDT-TTF)₂Cu(NCS)₂, the rapid oscillations at the edges of the figure are angle-dependent magnetoresistance oscillations (AMROs). The fine lines superimposed on the λ -(BETS)₂GaCl₄ data show how the full width of the peak is defined.

In order to obtain a quantitative estimate of t_\perp , it is necessary to use reliable values of v_\parallel [28, 30]. Figure 3(b) suggests that when the in-plane magnetic field is close to the \mathbf{a}^* -direction, it is likely that *both* Q1D and Q2D Fermi-surface sections will be able to support closed orbits; conversely, when the magnetic field is well away from this orientation, only the Q2D cylinder will be able to support closed orbits. As most of the accurate information deduced from the experiments in the previous sections concerns the Q2D Fermi-surface section, we concentrate on the range of ϕ over which it alone will determine the peak at $\theta = 90^\circ$.

We assume an effective-mass-tensor approximation for the in-plane motion on the Q2D Fermi-surface section [1]:

$$E = \frac{\hbar^2 k_x^2}{2m_1} + \frac{\hbar^2 k_y^2}{2m_2}. \quad (6)$$

Here m_1 and m_2 are effective masses *for linear motion* in the x - and y -directions. The cyclotron effective mass in such an approximation is $m^* = (m_1 m_2)^{1/2}$ [31]. Using the lengths of the axes of the elliptical cross-section of the Q2D Fermi-surface section derived from the AMROs

⁶ Alternative methods, such as the fitting of more complex functions to the background magnetoresistance and peak yielded negligible gains in accuracy and reproducibility, and were more time-consuming.

(2.43 nm⁻¹ and 0.815 nm⁻¹; see the previous section—we have divided by 2 to account for apparent doubling of the unit-cell height) and $m^* = 3.6 m_e$ (table 1), we obtain

$$\frac{m_1}{m_2} = \left(\frac{2.43}{0.815} \right)^2 \quad \text{and} \quad m_1 m_2 = (3.6 m_e)^2 = 12.96 m_e^2$$

yielding $m_1 = 10.73 m_e$, $m_2 = 1.207 m_e$ and $E_F \approx 20.95$ meV (cf. $m_1 = 10.59 m_e$, $m_2 = 1.177 m_e$ and $E_F \approx 18.4$ meV for κ -(BEDT-TTF)₂Cu(NCS)₂ [30]). Hence, using $\hbar \mathbf{v} = \nabla_{\mathbf{k}} E(\mathbf{k})$ [31], and the constraint $E = E_F$, the velocities $v_{\parallel}(\phi)$ may be derived for the Q2D Fermi-surface section.

The widths 2Δ derived from data such as those in figure 4 are plotted as a function of ϕ in figure 5. The figure also shows the prediction of equation (4) using v_{\parallel} derived from equation (6); the only fit parameter is t_{\perp} (see equation (5)). We have chosen to fit data for ranges of ϕ at which the Q2D pocket is expected to be the *sole* provider of closed orbits for in-plane magnetic fields; i.e. we avoided field orientations close to $-\mathbf{a}^*$ ($\phi = 90^\circ$) and \mathbf{a}^* ($\phi = 270^\circ$) (dashed lines) at which the Q1D sheets might also be expected to provide closed orbits in an in-plane field (see figure 3(b)). (Note that the experimental data show a strong peak close to $\phi = 90^\circ$ and 270° (instead of the minimum predicted by the model) suggesting that the Q1D sections are indeed the dominant cause of the peak in ρ_{zz} at these orientations.) The fit yields $v_{\perp} \approx 1200$ m s⁻¹, so⁷ $t_{\perp} \approx 0.21$ meV. A similar procedure has been carried out for κ -(BEDT-TTF)₂Cu(NCS)₂, giving an interplane transfer integral of $t_{\perp} \approx 0.04$ meV [30]. Therefore, the interplane transfer integral of λ -(BETS)₂GaCl₄ is a factor ~ 5 bigger than that in κ -(BEDT-TTF)₂Cu(NCS)₂.

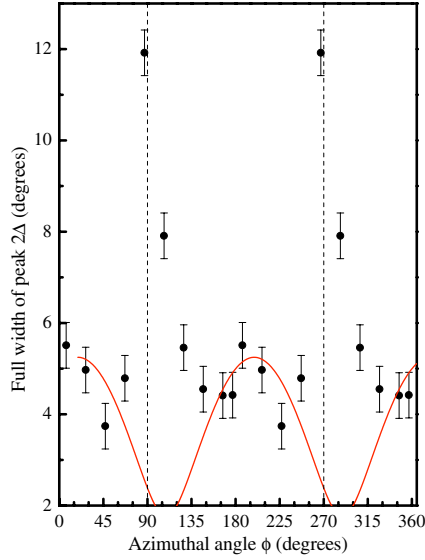


Figure 5. Full widths of peaks in ρ_{zz} close to $\theta = 90^\circ$ for λ -(BETS)₂GaCl₄ (points) plotted as a function of ϕ . The curve is given by equations (4), (5) and (6), with $t_{\perp} = 0.21$ meV. Note that we have chosen to fit data for ranges of ϕ at which the Q2D pocket is expected to be the *sole* provider of closed orbits for in-plane magnetic fields; i.e. we avoided field orientations close to $-\mathbf{a}^*$ ($\phi = 90^\circ$) and \mathbf{a}^* ($\phi = 270^\circ$) (dashed lines) at which the Q1D sheets might also be expected to provide closed orbits in an in-plane field (see figure 3(b))

⁷ The value $t_{\perp} = 0.21$ meV assumes that the interplane distance b which dominates the interlayer transport is that given by x-ray crystallography, 18.4 Å.

3.6. Summary

In summary, the magnetoresistance measurements indicate that the Fermi surface of λ -(BETS)₂GaCl₄ bears a strong resemblance to that of κ -(BEDT-TTF)₂Cu(NCS)₂ within the highly conducting Q2D planes. Moreover, the effective masses of the two salts are almost identical and the renormalizing interactions are probably of similar strength.

The width of the peak in the magnetoresistance close to $\theta = 90^\circ$ suggests that the interplane transfer integral of λ -(BETS)₂GaCl₄ is approximately five times bigger than that of κ -(BEDT-TTF)₂Cu(NCS)₂. This implies that λ -(BETS)₂GaCl₄ is a less two-dimensional material.

4. Penetration-depth measurements

4.1. Experimental details

In the current experiments, the penetration depth was inferred by placing the superconducting sample in a small coil which is the inductive element of a resonant tank circuit [32, 33]. The exclusion of flux from the sample, and hence the coil, decreases the inductance of the circuit; consequently the resonant angular frequency, $\omega = 1/\sqrt{LC}$, will increase. The well-known properties of inductors [34] lead to $\Delta A_\phi/A_C = \Delta L/L$, where ΔA_ϕ is the change in flux area, A_C is the area of the measurement coil, ΔL is the change in inductance and L is the total inductance. For small changes in inductance, $\Delta L/L_0 = 2 \Delta f/f_0$, where Δf is the change in resonant frequency f_0 is the initial resonant frequency and L_0 is the initial inductance. Through simple geometrical relations it can be shown that [35]

$$\frac{\Delta A_\phi}{A_C} = \frac{2r_s \Delta\lambda - \Delta\lambda^2}{R^2} \quad (7)$$

where $\Delta\lambda$ is the change in penetration depth, R is the effective radius of the coil, r_s is the effective sample radius. Simple estimates for the sample sizes used in the current experiments show that the second-order term is negligible [35], so

$$\Delta\lambda = \frac{R^2 \Delta f}{r_s f_0}. \quad (8)$$

The λ -(BETS)₂GaCl₄ samples used in the current study have a needle-like geometry [13]; a typical example had approximate dimensions $2 \times 0.170 \times 0.084$ mm³. In order to maximize the filling factor and cross-sectional area, the coil was made rectangular, with an effective area of 1.34 mm²; for the sample mentioned above, the effective sample radius is half the shortest dimension (0.042 mm) (note that the long axis of the crystal is perpendicular to the coil axis). Calibration was achieved by placing a spherical superconducting sphere of known size in the coil [2]. The sample was orientated in the coil such that the oscillating magnetic field was parallel to the crystallographic b^* -direction, i.e. perpendicular to the highly conducting planes [11]. The tank-circuit capacitance was provided by a 30 pF mica capacitor, and the circuit was driven at $f \approx 25$ MHz by a tunnel-diode oscillator [32]⁸. The sample and coil were placed in a ³He cryostat or dilution refrigerator. Quasistatic magnetic fields of up to 30 T were applied parallel to b^* .

Figure 6 shows $\Delta\lambda$ for a λ -(BETS)₂GaCl₄ crystal (deduced from the frequency of the tank circuit using equation (8)) as a function of temperature. The sharp rise in penetration between

⁸ It should be emphasized that this measurement technique represents a very weak perturbation of the sample. The radio-frequency (rf) magnetic field in the coil is ~ 1 μ T, several orders of magnitude smaller than typical applied fields. Moreover, the data were taken at a frequency of 25 MHz, whilst a BCS estimate of the pair-breaking frequency in λ -(BETS)₂GaCl₄ is ~ 160 GHz [35] i.e. the measurement frequency is insufficient to cause pair breaking.

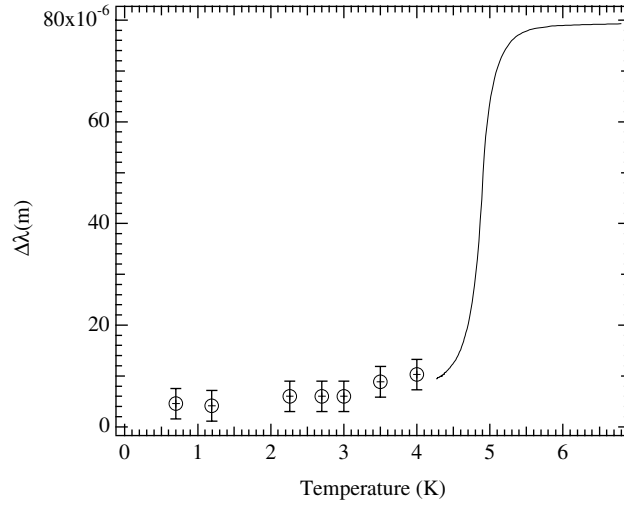


Figure 6. Change in penetration depth versus temperature at zero field in λ -(BETS)₂GaCl₄. Note that the cryostat used could only provide controlled, slow sweeps of temperature down to 4.2 K (data shown as a continuous curve). Below this, data are recorded at fixed, stable temperatures (points). The error bars on the points give typical uncertainties, valid across the whole temperature range shown.

4.5 K and 5.1 K gives a very clear indication of the superconducting-to-normal transition; above this temperature, $\Delta\lambda \approx 80 \mu\text{m}$ (i.e. comparable to the shortest dimension of the sample), indicating that the radio-frequency fields penetrate the whole crystal once it is in the normal state. This is in agreement with estimates of the low-temperature normal-state conductivity for λ -(BETS)₂GaCl₄ [12], which lead one to expect an in-plane skin depth $\delta \sim 100 \mu\text{m}$ [36, 37].

4.2. Measurements at low magnetic fields: determination of pinning parameters

Wu and Sridhar [38] have treated the repulsively interacting flux lines in a type-II superconductor as periodic, damped harmonic oscillator potentials modulated by a rf field. The physical justification of their model is that the repulsive interaction of the fluxoids causes the Abrikosov lattice [39, 40] to resist higher flux densities in a manner analogous to the way in which a two-dimensional network of springs resists compression. In such a model, the Labusch pinning potential parameter α corresponds to the restoring force on fluxoids displaced slightly by the current density J induced by the radio-frequency field [38]:

$$\eta \frac{dx}{dt} + \alpha x = \phi_0 J.$$

Here x is the fluxoid displacement, η is a damping parameter and ϕ_0 is the flux quantum [38]. In other words, a small perturbation displaces the fluxoid from its equilibrium position against the restoring force provided by the repulsion from neighbouring fluxoids and the pinning potential.

In the limit of small magnetic field ($H \ll B_{c2}$), the damping due to fluxoid viscous drag [38, 41] may be neglected, leading to a linear relationship between changes in the square of the penetration depth $\Delta\lambda^2$ and the magnetic induction B inside the sample [38]:

$$\Delta\lambda^2 = \frac{\phi_0}{\mu_0 \alpha(T)} B(H). \quad (9)$$

Figure 7 (inset) shows the field dependence of $\Delta\lambda^2$ at a temperature of $T = 700 \text{ mK}$. The

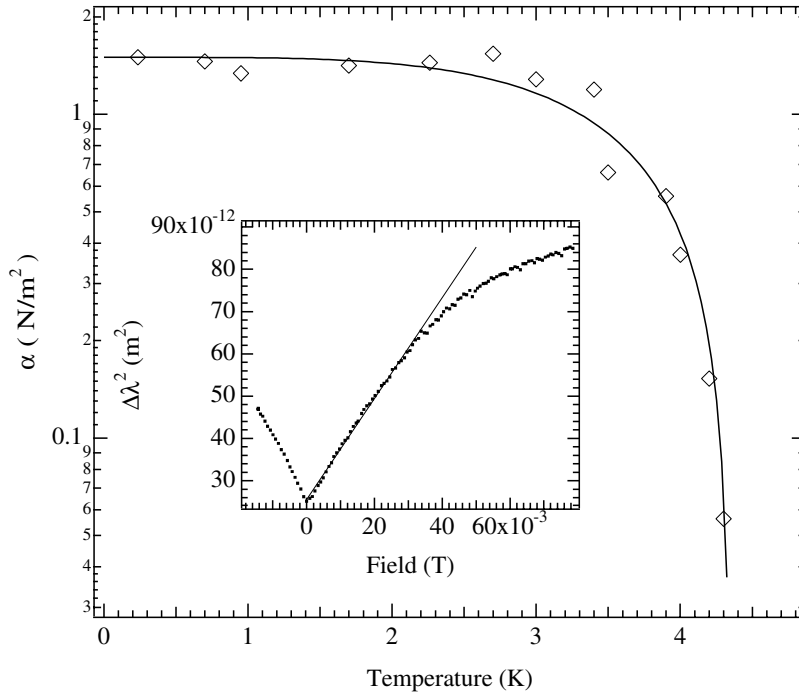


Figure 7. Inset: the determination of the Labusch parameter $\alpha(T)$ by a straight-line fit to low-field $\Delta\lambda^2$ versus $\mu_0 H$ data ($T = 700$ mK). Main figure: experimental values of α versus temperature (points); the curve is a fit to the two-fluid model expression.

sample is well inside the mixed state for fields above $\mu_0 H \approx 0.01$ T, so $B = \mu_0 H$; hence, the linear dependence predicted by equation (9) fits the data well, yielding a Labusch parameter of $\alpha(700 \text{ mK}) \approx 1.4 \text{ N m}^{-2}$.

Data similar to those in the inset of figure 7 were acquired at a range of temperatures; the resulting values of α are plotted in figure 7 (main figure) as a function of temperature. The solid-line fit through the data in figure 7 is the temperature dependence predicted from the two-fluid Gorter–Casimir [40, 42] model,

$$\alpha \propto \left[1 - \left(\frac{T}{T_c} \right)^4 \right]. \quad (10)$$

Figure 7 also highlights some of the differences between organic superconductors and the ‘high- T_c ’ cuprates. As $T \rightarrow 0$, the Labusch parameter of λ -(BETS) $_2$ GaCl $_4$ tends to 1.5 N m^{-2} , almost four orders of magnitude smaller than that of YBa $_2$ Cu $_3$ O $_7$ [38]. Moreover, whereas the two-fluid model is able to describe the λ -(BETS) $_2$ GaCl $_4$ data with a fair degree of accuracy, the pinning-force parameter of YBa $_2$ Cu $_3$ O $_7$ has been shown to follow the temperature dependence $(1 - (T/T_c)^2)^2$ [38].

4.3. Measurements at high magnetic fields: deviation from Campbell penetration-depth behaviour and the upper critical field

Figure 8 shows the measured change in penetration depth $\Delta\lambda$ for λ -(BETS) $_2$ GaCl $_4$ at intermediate fields and a temperature of 700 mK. $\Delta\lambda$ varies approximately as \sqrt{H} , as expected

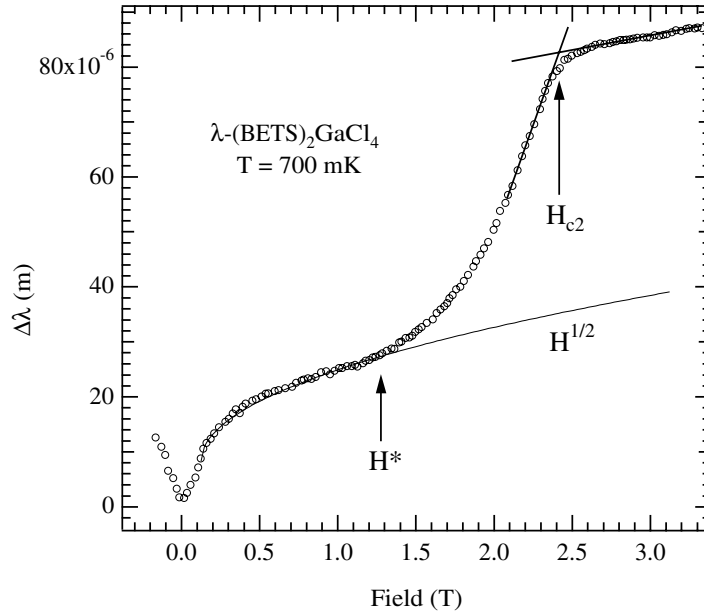


Figure 8. The change in penetration-depth signal versus field for λ -(BETS)₂GaCl₄ at 700 mK. The deviation from the Campbell penetration-depth behaviour is indicated as H^* while the saturation of the $\Delta\lambda$ signal indicates H_{c2} , determined from the straight-line intercepts.

in the Campbell scenario for fluxoid motion [38, 43]. However, above a field which we label $\mu_0 H^*$, $\Delta\lambda$ deviates from the \sqrt{H} dependence; this implies that the periodic harmonic well models [38, 44] are no longer applicable. At fields above $\mu_0 H^*$, $\Delta\lambda$ follows the approximate field dependence H^2 , until the penetration depth saturates.

The identification of the upper critical field in organic superconductors from conductivity data has been the subject of considerable debate [45, 46]; the transition is intrinsically broad, and phenomena such as a pronounced ‘hump’ in the resistivity and negative magnetoresistance are observed close to H_{c2} [1]. (Note that similar complications also afflict the ‘high- T_c ’ cuprates [47, 48].) Recently, a consensus has emerged whereby most of the transition region between zero resistance and normal-state magnetoresistance is regarded as a property of the mixed phase (see references [33, 46] and references therein); H_{c2} is then defined as the intersection of the extrapolations of the transition region and the normal-state magnetoresistance [33].

In penetration-depth measurements, the broadening is less severe since the measurement is not dependent on a macroscopic net current flow across the sample [38, 46]. The pinned fluxoids probed by rf fields do not experience as large an electric field gradient and hence the dissipation associated with the normal core is reduced [38, 46]. Nevertheless, the transition is still somewhat broadened, and so we follow the same spirit as the convention used in resistivity studies [33] and the GHz penetration-depth studies of reference [46], defining H_{c2} as the intersection of extrapolations of the penetration-depth curves below and above the point at which the saturation occurs (see figure 8). We can be confident that the saturated behaviour is characteristic of the normal state, as it continues up to at least 30 T without further features. This strongly suggests that the whole of the sample is penetrated by the rf fields in the normal state, as suggested in section 4.1.

The values of H_{c2} and H^* deduced from the penetration-depth measurements are shown as functions of temperature in figure 9. Four different λ -(BETS)₂GaCl₄ samples, taken from

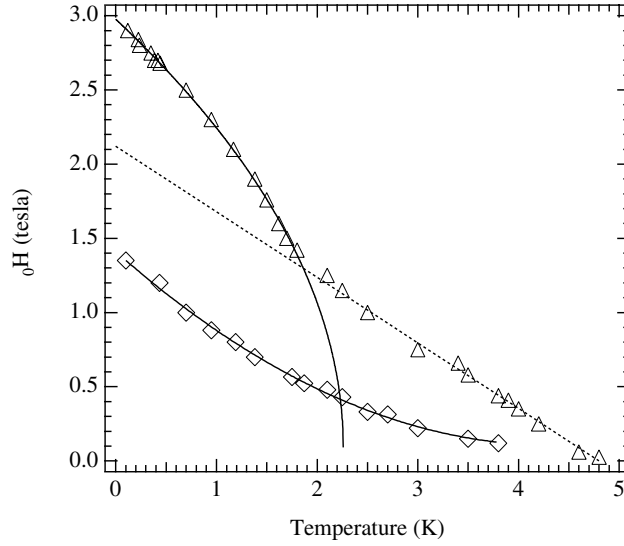


Figure 9. The notional phase diagram of λ -(BETS)₂GaCl₄ showing the upper critical field (triangles) and H^* , marking the inflection points in the penetration depth (diamonds). The quasistatic field is applied parallel to b^* , i.e. perpendicular to the quasi-two-dimensional planes of the sample. Points from four different samples are shown, often overlaying each other. The upper solid curve is $H_{c2} \propto (T^* - T)^{1/2}$; the dashed curve is $H_{c2} \propto (T_{c2} - T)$. The lower solid curve is a fit of the two-fluid model expression for the flux-line-lattice melting.

four separate growth batches, were used in the study. There were negligible differences in their behaviour, and the data from the four samples in figure 9 overlaid each other, suggesting that the characteristic fields measured are intrinsic properties of λ -(BETS)₂GaCl₄. We shall return to the temperature dependence of H_{c2} in a later section.

4.4. Flux-lattice melting at H^*

We now turn to the change in behaviour which occurs at the field H^* (see figure 8). We attribute the change at H^* to flux-line-lattice melting, as H^* follows the $(T_c - T)^2$ dependence expected from the Gorter–Casimir two-fluid model [42].

Additional support for this attribution comes from considering microscopic models of the melting process. Houghton *et al* [49] have considered the elastic moduli of the flux-line lattice and proposed that melting occurs when the mean thermal flux-line displacement $d(T)$ is a substantial fraction of the Abrikosov lattice parameter $\ell = (2\phi_0/\sqrt{3}B)^{1/2}$, i.e., $d(T) \approx c_L \ell$. Here c_L is the Lindemann parameter [50], a function used very generally in the description of solid–liquid transitions; typically $c_L \sim 0.1$ – 0.2 . The explicit expression for $d(T)$ is

$$d(T) = \sqrt{\frac{1}{2\pi} \left(\frac{G_i}{\gamma^2} \right)^{1/2} \frac{t}{(1-t)^{1/2}} \frac{b}{(1-b)} \left(\frac{4(\sqrt{2}-1)}{(1-b)^{1/2}} + 1 \right)} \ell^2 \quad (11)$$

where $t = T/T_c$ and $b = B/B_{c2}$. The parameter

$$G_i = (16\pi^3 \kappa^4 (k_B T)^2) / (\phi_0^3 H_{c2}(0))$$

describes the importance of fluctuations in a given system; γ is the anisotropy term defined by

$$\gamma \equiv \frac{\xi_{xy}}{\xi_z} \quad (12)$$

with ξ_{xy} and ξ_z being the in-plane and interplane coherence lengths respectively. κ is another Ginzburg–Landau parameter giving the ratio of penetration depth to the coherence length for a particular orientation [40, 49]. In this case we require $\kappa = \lambda/\xi_{\perp}$. Using Ginzburg–Landau theory in the limit⁹ $T \rightarrow 0$ yields $\xi_{\perp} \approx 1.4$ nm and $\lambda \approx 150$ nm for λ -(BETS)₂GaCl₄, resulting in $\kappa \approx 107$.

In this model, the melting field at each temperature can be interpreted as the point at which the product of c_L and the lattice spacing is roughly equal to the average flux-line displacement. Thus, an increasing field reduces the average intervortex spacing, thereby facilitating melting [49]. Substituting $\mu_0 H^* \approx 1$ T at $T = 700$ mK and $\kappa = 107$ into the above equations yields a flux-line displacement of approximately 6.0 nm, roughly 12% of the Abrikosov lattice spacing. This implies that $c_L \approx 0.12$, a value entirely typical of a solid–liquid transition [50].

In isotropic superconducting systems, the melting of the flux-line lattice occurs so close to H_{c2} as to be indistinguishable from it [40]. However, for materials such as λ -(BETS)₂GaCl₄ (and in κ -(BEDT-TTF)₂Cu(NCS)₂; see references [53, 56]), the large anisotropy of the superconducting properties permits the melting line to be observed over extended regions of the H – T phase diagram, well clear of H_{c2} .

5. Discussion: comparison of λ -(BETS)₂GaCl₄ with κ -(BEDT-TTF)₂Cu(NCS)₂; dimensional crossover

Having seen in section 3 that the Fermi surface of λ -(BETS)₂GaCl₄ and that of κ -(BEDT-TTF)₂Cu(NCS)₂ bear some striking similarities within the Q2D planes but have interplane transfer integrals differing by a factor ~ 5 , it is interesting to compare their superconducting properties.

The work of Belin *et al* [46] has shown that conventional resistivity measurements can yield unrepresentative values for the upper critical field of κ -(BEDT-TTF)₂Cu(NCS)₂ (see also [48, 58]); the difficulties result from the dissipative mechanisms mentioned in section 4.3, which act to broaden the resistive transition [1, 45]. Thermal conductivity, magnetization and penetration-depth measurements seem to be less susceptible to these problems and give a better reflection of the true H_{c2} [46]. We have therefore compiled the $H_{c2}(T)$ plot in figure 10 using available thermal conductivity [46], magnetization [53, 54] and MHz [52] and microwave (12–25 GHz) [46] penetration measurements. There is some scatter amongst the data from different measurements, but all suggest that $(\partial H_{c2}/\partial T)$ increases in magnitude as T increases, and in fact the power law $H_{c2} \propto (T_c - T)^{2/3}$ is quite successful in describing the data (figure 10).

A material made up of weakly coupled superconducting planes may transform from a three-dimensional system to what is in effect a series of two-dimensional superconductors as the interlayer coherence length decreases with decreasing temperature [60]. The dimensional crossover occurs when the interplane coherence length ξ_z becomes shorter than the interplane spacing of the quasi-two-dimensional layers. Muon-spin-rotation studies [55] have shown that this transition occurs in κ -(BEDT-TTF)₂Cu(NCS)₂ at magnetic fields ~ 7 mT, i.e. three orders of magnitude smaller than typical values of H_{c2} (figure 10). This strongly suggests that the variation of H_{c2} shown in figure 10 is typical of a quasi-two-dimensional superconductor consisting of weakly coupled layers [53, 56, 59].

⁹ This procedure was carried out using equations (12), (13) and (14) in the limit $T \rightarrow 0$ [51]. See section 5 for a discussion of some of the difficulties inherent in this procedure.

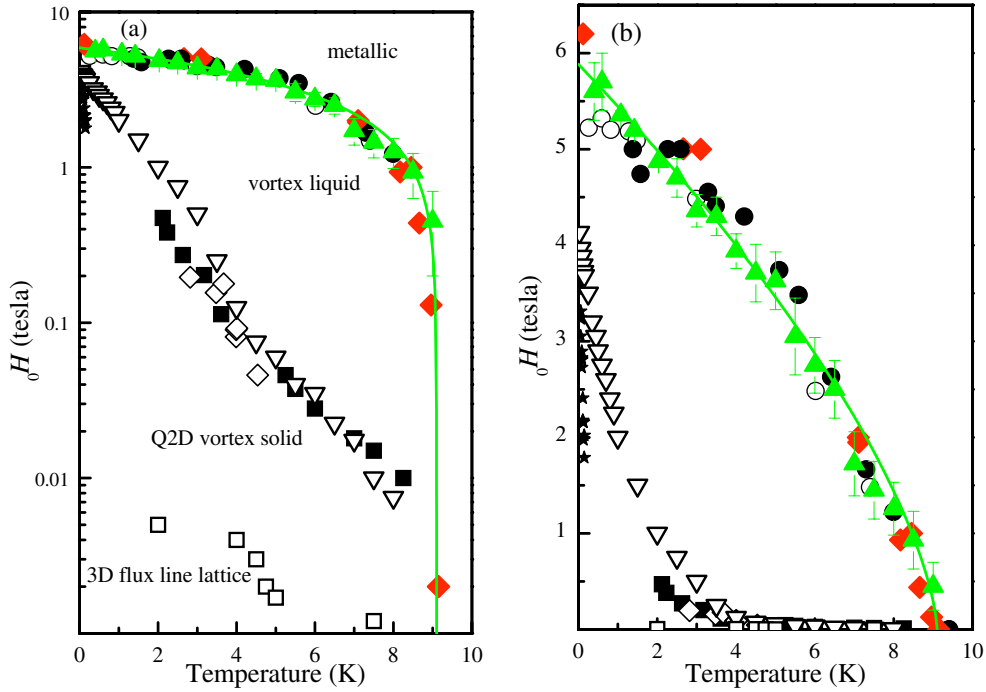


Figure 10. Critical fields in κ -(BEDT-TTF)₂Cu(NCS)₂, plotted on logarithmic (a) and linear (b) field scales. The data for H_{c2} comprise filled triangles (MHz penetration data obtained using the apparatus described in the current paper [52]), filled circles (microwave penetration studies; reference [46]; errors in values of $\mu_0 H_{c2}$ typically ± 0.5 T), open circles (thermal conductivity data from reference [46]; errors not given) and shaded diamonds (magnetization data; the lowest-temperature point was determined by examining the attenuation of de Haas–van Alphen oscillations [53] and the higher-temperature points are from the scaling studies in reference [54]). The solid curve is proportional to $(T_c - T)^{2/3}$, with $T_c = 9.1$ K. The triangles show the irreversibility field from magnetization [53]; the filled squares and stars represent 2D melting from magnetometry and GHz studies [56] (see also the NMR data of reference [57]). The hollow squares are from muon-spin-rotation studies [55] and denote the 3D–2D transition.

Figure 9 shows that the upper critical field of λ -(BETS)₂GaCl₄ (conducting planes perpendicular to the applied magnetic field) has a linear region $H_{c2} \propto (T_c - T)$ that spans from T_c to approximately 1.9 K. Below 1.9 K, a definite change in the slope of the upper critical field occurs, and H_{c2} begins to follow the power law $H_{c2} \propto (T^* - T)^\zeta$, with T^* a fit parameter; powers ζ in the range 0.5–0.7 provide an adequate fit to the data.

The behaviour of H_{c2} in λ -(BETS)₂GaCl₄ at temperatures below 1.9 K is therefore very similar to that of H_{c2} in κ -(BEDT-TTF)₂Cu(NCS)₂ over the whole temperature range shown in figure 10, and is thus characteristic of a two-dimensional superconductor with weakly coupled layers [56, 59]. On the other hand, the linear variation of H_{c2} in λ -(BETS)₂GaCl₄ at higher temperatures follows the expectations of Ginzburg–Landau theory for three-dimensional superconductors [40, 63]. We therefore attribute the change in gradient at 1.9 K to dimensional crossover from quasi-two-dimensional (low temperatures) to three-dimensional (high temperatures). As we shall now show, this is entirely consistent with estimates of the interplane coherence length in λ -(BETS)₂GaCl₄.

The dependence on the magnetic field orientation of B_{c2} [35] in λ -(BETS)₂GaCl₄ is qualitatively similar to the predictions of the Ginzburg–Landau anisotropic effective-mass

approximation [40, 61, 62, 64]

$$B_{c2}(\theta) = \frac{B_{c2}(\theta = 0)}{\sqrt{\cos^2(\theta) + \gamma^{-2} \sin^2(\theta)}} \quad (13)$$

where θ is the angle between \mathbf{b}^* and the applied magnetic field and γ has been defined in equation (12). Using Ginzburg–Landau theory [40], the in-plane coherence length may be estimated from the upper critical field when the magnetic field is parallel to \mathbf{b}^* :

$$H_{c2}(\theta = 0) = \frac{\phi_0}{2\pi \xi_{xy}^2}. \quad (14)$$

Fits of the θ -dependence of H_{c2} at $T = 1.75$ K [51, 64] (the temperature at which the change in gradient in figure 9 occurs) yield $\xi_z \approx 1.85$ nm, almost identical with the interplane spacing, and supporting our assertion that the change in gradient in figure 9 at 1.9 K is associated with a dimensional crossover.

Dimensional crossovers with the magnetic field applied perpendicular to the Q2D planes have been observed in artificial Q2D superconducting structures [65, 66] and in organic superconductors such as κ -(BEDT-TTF)₂Cu(NCS)₂ [55, 56]; however, in the majority of these cases, the effect of the crossover is observed at magnetic fields less than H_{c2} . λ -(BETS)₂GaCl₄ is perhaps unique in providing the correct anisotropy for the crossover to be observed in the behaviour of $H_{c2}(T)$.

In section 3.5 we demonstrated that the interplane transfer integral of λ -(BETS)₂GaCl₄ is a factor ~ 5 larger than that of κ -(BEDT-TTF)₂Cu(NCS)₂. The greater ‘three-dimensionality’ of the band structure of λ -(BETS)₂GaCl₄ compared to κ -(BEDT-TTF)₂Cu(NCS)₂ obviously manifests itself in the superconducting behaviour (compare figures 9 and 10); whereas λ -(BETS)₂GaCl₄ exhibits 2D–3D dimensional crossover in its $H_{c2}(T)$ behaviour, $H_{c2}(T)$ in κ -(BEDT-TTF)₂Cu(NCS)₂ is entirely characteristic of a Q2D superconductor.

6. Summary

In summary, we have measured the Fermi-surface topology of the organic superconductor λ -(BETS)₂GaCl₄ using Shubnikov–de Haas and angle-dependent magnetoresistance oscillations. The data show that the Fermi-surface topology of λ -(BETS)₂GaCl₄ is very similar indeed to that of the most heavily studied organic superconductor, κ -(BEDT-TTF)₂Cu(NCS)₂, except in one important respect; the interplane transfer integral of λ -(BETS)₂GaCl₄ is a factor ~ 5 larger than that in κ -(BEDT-TTF)₂Cu(NCS)₂. The increased three-dimensionality of λ -(BETS)₂GaCl₄ is manifested in radio-frequency penetration-depth measurements, which show a clear dimensional crossover in the behaviour of H_{c2} . The radio-frequency measurements have also been used to extract the Labusch parameter determining the fluxoid interactions as a function of temperature, and to map the flux-lattice melting curve.

We have observed a discrepancy between the angle-dependent magnetoresistance oscillation and Shubnikov–de Haas data which suggests that the true unit-cell height at low temperatures is double that inferred from x-ray studies. At present, this has not been detected by other techniques.

It is interesting to note that the anisotropies and Ginzburg–Landau parameters of the organic superconductors λ -(BETS)₂GaCl₄ (this work) and κ -(BEDT-TTF)₂Cu(NCS)₂ [53, 55, 56] span the typical values found in ‘high- T_c ’ cuprates such as YBCO and BISCCO [40]. However, as the current work has shown, in contrast to the case for the cuprates, the Fermi-surface topologies and complete phase diagrams of organic superconductors such as λ -(BETS)₂GaCl₄ and κ -(BEDT-TTF)₂Cu(NCS)₂ can be mapped out in detail using accessible

laboratory fields. Moreover, details of the band structure in the organics can be related directly to the superconducting properties. The availability of a large number of organic superconductors of varying dimensionality and band structure [1, 23] should potentially allow very stringent experimental tests of models of superconductivity in layered materials to be carried out.

Acknowledgments

This work was supported by the Department of Energy, the National Science Foundation (NSF), the State of Florida and EPSRC (UK). Acknowledgement is made to the donors of The Petroleum Research Fund, administered by the ACS, for partial support of this research. CHM thanks J S Brooks for very useful insights into the radio-frequency measurement technique. We are grateful to Stephen Hill and Monty Mola for their considerable help in compiling figure 10 and Kazumi Maki, Ross McKenzie and Stephen Blundell for illuminating discussions. Paul Goddard, Mike Whangbo and J-H Koo are thanked for permission to use data and calculations from references [15, 30] prior to publication. We also thank Akiko Kobayashi for recording the 17 K x-ray structure upon which the bandstructure calculations shown in figure 3(b) are based. Finally, we acknowledge the suggestions of one of the referees, which have helped to clarify several points.

Appendix. A note on the radio-frequency response

In the current paper we have extracted parameters which describe the superconducting state of λ -(BETS)₂GaCl₄ under the assumption that all of the apparent changes in the penetration of the radio-frequency field are due to the variation of λ . It is therefore very important to assess whether this assumption is valid. Moreover, as little has been written in the literature about the radio-frequency techniques employed, it is useful to summarize the artefacts which can affect the experimental data. For future reference, we hope that it is also useful to provide estimates of some of the parameters used in the theory used to model experimental data [44].

Coffey and Clem [44] have treated the behaviour of a superconductor in a rf field over a broad frequency range. Using their approach, the contributions to the penetration-depth signal from surface-impedance and skin-depth effects can be evaluated as the temperature or applied magnetic field are varied. The model defines boundaries at which the surface-impedance and skin-depth effects become non-negligible; these are set by evaluating the flux creep factor [44].

The flux creep factor ε is determined by ν , the ratio of the fluxoid barrier height U_0 to the typical thermal energy $k_B T$, $\nu = U_0/(2k_B T)$. The flux creep factor is then determined by $\varepsilon = 1/I_0(\nu)^2$, where I_0 is a zeroth-order modified Bessel function of the first kind [44]. ε parametrizes the degree to which thermal effects assist the motion of fluxoids.

In the limit of large ε (i.e. $\varepsilon \sim 1$), thermal excitation causes the behaviour of fluxoids to approach that of completely unpinned fluxoids. In this case, the complex effective resistivity ($\tilde{\rho}_v(\omega)$) becomes a factor contributing to the measured change in penetration depth. $\tilde{\rho}_v(\omega)$ [44] is given by the expression

$$\tilde{\rho}_v(\omega) = \frac{\varepsilon + (\omega\tau)^2 + i(1 - \varepsilon)\omega\tau}{1 + (\omega\tau)^2} \rho_f \quad (\text{A.1})$$

where $\rho_f = B\phi_0/\eta$ is the flux flow resistivity and $\omega\tau$ represents the product of the measurement frequency and the relaxation time of the normal-state quasiparticles.

An order-of-magnitude estimate of U_0 is given by considering the energy at which the

harmonic oscillator potentials of neighbouring fluxoids cross, yielding [38]

$$U_0 \approx \frac{2}{\pi^2} \alpha L^3.$$

The characteristic length L [38] will be roughly equal to the Abrikosov lattice spacing, $L = \ell$, so the pinning-well barrier height U_0 can be estimated using

$$U_0 = \frac{2\alpha}{\pi^2} \left(\frac{2}{\sqrt{3}} \frac{\phi_0}{B} \right)^{3/2}. \quad (\text{A.2})$$

Equation (A.2) shows that U_0 decreases as the field B increases, so the surface-impedance and skin-depth effects will be most prominent at high magnetic fields. Within the superconducting state, the highest field (i.e. worst-case scenario) at which we make quantitative deductions about vortex behaviour is $\mu_0 H^*$, the field at which the penetration depth indicates a divergence from the Campbell regime. Substituting the value for 700 mK, we obtain $U_0 \sim 16$ K. At this field and temperature, $\nu \sim 4$, leading to $\varepsilon \sim 0.005$.

Equation (A.1) also shows that the value of $\omega\tau$ contributes to the complex resistivity. Taking a frequency $\omega/2\pi \approx 25$ MHz from the current experiments and τ from measurements of the normal-state resistivity [12] (or the penetration depth: see figure 6), we obtain $\omega\tau \sim 0.005$. Therefore, the fact that both ε and $\omega\tau$ are $\ll 1$ indicates that the surface-impedance and skin-depth effects have negligible impact [44] on the experiments on λ -(BETS)₂GaCl₄ reported in this work.

Appendix B. References

- [1] Singleton J 2000 *Rep. Prog. Phys.* **63** 1111
- [2] Carrington A, Bonalde I J, Prozorov R, Gianetta R W, Kini A M, Schlueter J, Wang H H, Geiser U and Williams J M 1999 *Phys. Rev. Lett.* **83** 4172
- [3] Elsinger H, Wosnitzer J, Wanka S, Hagel J, Schweitzer D and Strunz W 2000 *Phys. Rev. Lett.* **84** 6098
- [4] Ichimura K *et al* 1999 *Synth. Met.* **103** 1812
Ichimura K *et al* 1999 *J. Supercond.* **12** 519
Arai T *et al* 2001 *Phys. Rev. B* **63** 104518
- [5] Lefebvre S, Wzietek P, Brown S, Bourbonnais C, Jerome D, Meziere C, Fourmigue M and Batail P 2000 *Phys. Rev. Lett.* **85** 5420
- [6] Schmalian J 1998 *Phys. Rev. Lett.* **81** 4232
- [7] Kuroki K and Aoki H 1999 *Phys. Rev. B* **60** 3060
- [8] Maki K, Puchkaryov E and Won H 1999 *Synth. Met.* **103** 1933
- [9] Louati R, Charfi-Kaddour S, Ben Ali A, Bennaceau R and Heritier M 1999 *Synth. Met.* **103** 1857
- [10] Kato R, Kobayashi H and Kobayashi A 1991 *Synth. Met.* **42** 2093
- [11] Montgomery L K, Burgin T, Huffman J C, Carlson K D, Dudek J D, Yanconi G A, Menga L A, Mobley P R, Kwok W K, Williams J M, Schirber J E, Overmyer D L, Ren J, Rovira C and Wangbo M-H 1993 *Synth. Met.* **56** 2090
- [12] Montgomery L K, Burgin T, Huffman J C, Ren J and Whangbo M-H 1994 *Physica C* **219** 490
- [13] Kobayashi H, Udagawa T, Tomita H, Bun K, Naito T and Kobayashi A 1993 *Chem. Lett.* **1993** 1559
- [14] Uji *et al* have recently observed what is believed to be magnetic field-induced superconductivity in λ -(BETS)₂FeCl₄; see Uji S *et al* 2001 *Nature* **410** 908
However, this salt is not a superconductor at zero field.
- [15] Whangbo M-H and Koo H-J 2001 unpublished calculations based on x-ray structure data recorded at a temperature of 17 K by Akiko Kobayashi
- [16] Montgomery L K, Burgin T, Miebach T, Dunham D and Huffman J C 1996 *Mol. Cryst. Liq. Cryst.* **284** 73
- [17] Herlach F 1999 *Rep. Prog. Phys.* **62** 859
- [18] House A A, Harrison N, Blundell S J, Deckers I, Singleton J, Herlach F, Hayes W, Perenboom J A A J, Kurmoo M and Day P 1996 *Phys. Rev. B* **53** 9127
- [19] Nam M S, Blundell S J, Ardavan A, Symington J A and Singleton J 2001 *J. Phys.: Condens. Matter* **13** 2271
- [20] Shoenberg D 1984 *Magnetic Oscillations in Metals* (Cambridge: Cambridge University Press)

- [21] Caulfield J M, Lubczynski W, Pratt F L, Singleton J, Ko D Y K, Hayes W, Kurmoo M and Day P 1994 *J. Phys.: Condens. Matter* **6** 2911
- [22] Quader K F, Bedell K S and Brown G E 1987 *Phys. Rev. B* **36** 156
Leggett A J 1968 *Ann. Phys., NY* **46** 76
Kohn W 1961 *Phys. Rev.* **123** 1242
Kanki K and Yamada K 1997 *J. Phys. Soc. Japan* **66** 1103
- [23] Wosnitzer J 1996 *Fermi Surfaces of Low-Dimensional Organic Metals and Superconductors* (Berlin: Springer)
- [24] Mielke C H, Harrison N, Rickel D G, Lacerda A H, Vestal R M and Montgomery L K 1997 *Phys. Rev. B* **56** R4309
- [25] Harrison N, Rzepniewski E, Singleton J, Gee P J, Honold M M, Day P and Kurmoo M 1999 *J. Phys.: Condens. Matter* **11** 7227
- [26] Montgomery L K and Huffman J C 2001 unpublished results
- [27] For a discussion of the issue of interplane dispersion in quasi-two-dimensional metals and measurements such as this one, see
Moses P and McKenzie R H 1999 *Phys. Rev. B* **60** 7998
Yoshioka D 1995 *J. Phys. Soc. Japan* **64** 3168
McKenzie R H and Moses P 1998 *Phys. Rev. Lett.* **81** 4492
McKenzie R H and Moses P 1999 *Phys. Rev. B* **60** 11 241
- [28] Osada T *et al* 1996 *Phys. Rev. Lett.* **77** 5261
Hanasaki N *et al* 1998 *Phys. Rev. B* **57** 1336
Hanasaki N *et al* 1999 *Phys. Rev. B* **60** 11 210
- [29] Others propose that 'self-crossing orbits' are more effective than closed orbits in averaging v_{\perp} ; however, the geometrical constraints on the peak in ρ_{zz} are identical. See
Peschansky V G and Kartsovnik M V 1999 *Phys. Rev. B* **60** 11 207
Lee I J and Naughton M J 1998 *Phys. Rev. B* **57** 7423
- [30] Singleton J, Goddard P A, Ardavan A, Harrison N, Blundell S J, Schlueter J A and Kini A M 2001 *Phys. Rev. Lett.* submitted
(Singleton J, Goddard P A, Ardavan A, Harrison N, Blundell S J, Schlueter J A and Kini A M 2001 *Preprint cond-mat/0104570*)
Goddard P, Ardavan A, Singleton J and Schlueter J A 2001 to be published
- [31] Ashcroft N W and Mermin N D 1976 *Solid State Physics* (New York: Holt-Saunders)
- [32] VanDeGrift C T 1975 *Rev. Sci. Instrum.* **46** 599
VanDeGrift C T and Love D P 1981 *Rev. Sci. Instrum.* **52** 712
- [33] Singleton J, Symington J A, Nam M S, Ardavan A, Kurmoo M and Day P 2000 *J. Phys.: Condens. Matter* **12** L641
- [34] See e.g.
Bleaney B I and Bleaney B 1990 *Electricity and Magnetism* 3rd edn (Oxford: Oxford University Press)
- [35] Mielke C H 1996 *PhD Thesis* Clark University, Worcester, MA
- [36] Schrama J M, Singleton J, Edwards R S, Ardavan A, Rzepniewski E, Harris R, Goy P, Gross M, Schlueter J, Kurmoo M and Day P 2001 *J. Phys.: Condens. Matter* **13** 2235
- [37] Hill S 2000 *Phys. Rev. B* **62** 8699
- [38] Wu D and Sridhar S 1990 *Phys. Rev. Lett.* **65** 2074
- [39] Abrikosov A A 1957 *Zh. Eksp. Teor. Fiz.* **32** 1442
- [40] Tinkham M 1996 *Introduction to Superconductivity* 2nd edn (New York: McGraw-Hill)
- [41] Bardeen J and Stephen M J 1965 *Phys. Rev.* **140** A1197
- [42] Gorter C J and Casimir H B G 1934 *Phys. Z.* **35** 963
- [43] Campbell A M and Evetts J E 1972 *Adv. Phys.* **21** 199
- [44] Coffey M W and Clem J R 1991 *Phys. Rev. Lett.* **67** 386
- [45] Ito H, Ishiguro T, Komatsu T, Saito G and Anzai H 1994 *Physica B* **201** 470 and references therein
Ishiguro T, Ito H, Sushko Yu V, Otsuka A and Saito G 1994 *Physica B* **197** 563
Zuo F, Su X, Zhang P, Schlueter J A, Kelly M E and Williams J M 1998 *Phys. Rev. B* **57** R5610
Zuo F, Schlueter J A, Kelly M E and Williams J M 1996 *Phys. Rev. B* **54** 11 973
- [46] Belin S, Shibauchi T, Behnia K and Tamegai T 1999 *J. Supercond.* **12** 497
- [47] Finnemore D K 1992 *Phenomenology and Applications of High Temperature Superconductors* (Reading, MA: Addison-Wesley) pp 164
- [48] Ando Y, Boeinger G S, Passner A, Schneemeyer L F, Kimura T, Okuya M, Watauchi S, Shimoyama J, Kishio K, Tamasaku K, Ichikawa N and Uchida S 1999 *Phys. Rev. B* **60** 12 475 and references therein
- [49] Houghton A, Pelcovits R A and Sudbo A 1989 *Phys. Rev. B* **40** 463

- [50] See e.g. Ziman J M 1972 *Principles of the Theory of Solids* 2nd edn (Cambridge: Cambridge University Press) and references therein
- [51] Mielke C H *et al* 2001 to be published
- [52] Singleton J and Mielke C H 2001 *Contemp. Phys.* submitted
- [53] Sasaki T, Biberacher W, Neumaier K, Hehn W, Andres K and Fukase T 1998 *Phys. Rev. B* **57** 10 889
- [54] Lang M, Steglich F, Toyota N and Sasaki T 1994 *Phys. Rev. B* **49** 15 227
- [55] Lee S L, Pratt F L, Blundell S J, Aegerter C M, Pattenden P A, Chow K H, Forgan E M, Sasaki T, Hayes W and Keller H 1997 *Phys. Rev. Lett.* **79** 1563
- [56] Mola M, Hill S, Brooks J S and Qualls J S 2001 *Phys. Rev. Lett.* **86** 2130
- [57] Mayaffre H, Wzietek P, Jerome D and Bazovskii S 1996 *Phys. Rev. Lett.* **76** 4951
- [58] See Graebner J E, Haddon R C, Chichester S V and Glarum S H 1990 *Phys. Rev. B* **41** 4808 and references therein
- [59] A similar curvature in H_{c2} versus T data has been observed in artificially constructed 2D superconductors (Mo–Ge films of thickness ~ 2 nm; the field was applied perpendicular to the 2D planes), suggesting that it is a generic property of 2D superconductors; see Graybeal J M and Beasley M R 1984 *Phys. Rev. B* **29** 4167
- [60] Lawrence W E and Doniach S 1970 *Proc. 12th Int. Conf. on Low Temp. Phys. (Kyoto)* ed E Kanda, p 361
- [61] Nakamura T, Komatsu T, Saito G, Osada T, Kagoshima S, Miura N, Kato K, Maruyama Y and Oshima K 1993 *J. Phys. Soc. Japan* **62** 4373
- [62] Morris R C, Coleman R V and Bhandari R 1972 *Phys. Rev. B* **5** 895
- [63] Parks R D (ed) 1969 *Superconductivity* (New York: Dekker)
- [64] A number of authors have compared the magnetic field orientation dependence of H_{c2} in organic superconductors with various theoretical expressions. It is found that the Ginzburg–Landau effective-mass expressions fit the data reasonably well for angles away from $\theta = 90^\circ$. However, close to in-plane magnetic fields ($\theta = 90^\circ$), mechanisms limited by spin (rather than orbital) effects take over, so a simple ratio of the in-plane H_{c2} to the perpendicular H_{c2} is NOT a reliable guide to the relative sizes of the coherence lengths. This point is discussed at some length in reference [1] in Nam M-S *et al* 1999 *J. Phys.: Condens. Matter* **11** L477 and in reference [33] and references cited in these papers. In reference [51] these problematic orientations are deliberately avoided.
- [65] White W R, Kapitulnik A and Beasley M R 1991 *Phys. Rev. Lett.* **66** 2826
- [66] The majority of dimensional crossover studies employing artificial layered structures focus on the effect of an in-plane magnetic field, which is not relevant in the current context; see e.g. Ruggiero S T, Barbee T W and Beasley M R 1980 *Phys. Rev. Lett.* **45** 1299 and references therein